JOURNAL OF MATERIALS SCIENCE 23 (1988) 3421–3434

Dynamic crack propagation in rubber-modified composite models

G. A. PAPADOPOULOS, G. C. PAPANICOLAOU
Department of Engineering Science, Section of Mechanics, The National Technical University of Athens, 5, Heroes of Polytechnion Avenue, GR-15773 Athens, Greece

The dynamic crack propagation behaviour of several rubber-modified composite models has been studied. In all cases the method of high speed photography along with the method of dynamic caustics was used. Results of crack propagation mode observation, fracture toughness and crack propagation velocity measurements are presented here. Especially in the case of two "complex" inclusions it was found that the crack propagation mode is highly rate dependent. At low test rates the crack growth tends to follow an almost straight crack path while an increase in strain rate in general results in the formation of a kink in the interparticle area. In the same area a crack propagation delay, and in some cases arrest, was observed while both the crack propagation velocity v and dynamic stress intensity factor K_I^d showed an intense variation. For the sake of comparison, specimens with one and/or two press-fitting inclusions as well as with two holes were fractured under dynamic loads. In all cases both qualitative and quantitative results were obtained.

1. Introduction

It is well known that brittle polymers can be toughened by the addition of small amounts of rubber particles [1, 2]. The most common technique usually followed for the production of rubber-modified plastics is to resolve rubber as a separate phase which may incorporate inclusions of the polymer. Recently some attempts have been made to toughen thermoplastics by blending with recycled rubber crumb [3–5].

There are several types of rubber particle structure. Among them the most common are the "core shell" and the "onion" structure. In the former type, each polymer inclusion is surrounded by a concentric thin spherical shell of rubber; while in the "onion" structure there are several concentric spheres of rubber and polymer [6–9].

The role of the toughening mechanisms encountered in rubber-modified plastics is to dissipate strain energy that would otherwise be available to extend an existing flow or crack. Toughening mechanisms include shear yielding and crazing, interaction between them and finally diversion and multiplication of a growing crack. Since the rubber is incompressible having a Poisson's ratio of about 0.5, a dilatational stress field is developed at the plastic–rubber interface as a result of which the development of crazing is encouraged. Crazing is developed in a direction perpendicular to that of the applied stress and initiated at the rubber–matrix interface. The smaller the interparticle distance, the higher the craze density and thus the higher the ultimate tracture energy.

The structure of crazes is distinct from that of the bulk polymer: it is porous, with a void content of about 40% [10] and the polymer chains are partially aligned parallel to the load [11, 12]. As the crazes are weaker than the bulk they provide sites for the initiation of fracture. Crack propagation occurs by the continued formations and rupture of crazed material.

However crazing is not the only toughening mechanism encountered in rubber-modified polymers. Various theories have been proposed to explain fracture toughness of two-phase polymers. Observations of stress-whitening and density decreases on straining in HIPS led Merz *et al.* [13] to the suggestion that many small cracks were formed on straining but the rubber particles spanned the cracks and hindered further crack growth. The same authors showed that optimum toughness corresponds to a specific size of the rubber domains existing in the material. An alternate energy-absorption mechanism has been proposed in [14] according to which rubber particles act as stress concentrators so that many microcracks are developed around them. Also, it was postulated that rubber particles act as crack stoppers while due to their ability to absorb a great deal of energy when stretched higher fracture energies are required. Next, according to the theory developed in [15], rubber particles induce triaxial tension under the influence of which the T_g of the matrix material is lowered sufficiently to permit facile cold-drawing and shear yielding.

Another important factor which determines the fracture toughness of rubber-modified polymers is the rubber particle size. Various theories have been concerned with particle size. However, some of them indicate an increase in toughness with a respective increase in particle size [16–17] while other studies suggest an increase in toughness with a decrease in particle size [17, 18]. Each of these cases is understandable using the model described in [19]. According to this model there is a maximum probable impact

0022–2461/88 $03.00 + .12

strength at a specific particle size that depends on the graft level required to achieve compatibility between the two phases. Particle size may affect fracture in another way. More specifically, during the crack propagation process a plastic zone is developed at the tip of the crack the size of which depends on the type of the material. If the particle size is small compared to the size of the plastic zone then the particle size does not affect the continuum aspects of the fracture process. However, since the size of the plastic zone is changed during the crack propagation process, there is an overall effect of the particles on the relaxation spectrum of the material. The effect of the particles on the time-dependence response characteristics is more pronounced when particles are large compared to the size of the plastic zone developed at the tip of the crack since in that case there is a strong stress interaction between the tip of the advancing crack and the filler particles.

In addition, the nature of the interfacial bond between matrix and particles is of crucial importance. In fact, perfect adhesion corresponding to continuity of stresses and displacements at the interface is a most common assumption for analytical treatments. However, with real composites, this condition is very seldom fulfilled. The morphology of rubber-modified polymers is expected to be quite complex. Rubber–matrix interfaces and/or interphases may be involved [19]. Also as it is well known, in the region between matrix and filler a third phase is developed consisting of areas of imperfect adhesion, stress concentrations, microcracks, impurities and other defects [20–28]. The microcracks developed in this third phase are centres from which failure almost always begins. The rate of crack growth depends strongly on the degree of inhomogeneity of the material not only in the macroscopic sense of the term, but rather on its microscopic sense. This means that if we consider the composite as being macroscopically homogeneous, the factor upon which the rate of crack growth depends is the microscopic inhomogeneity which characterizes the region surrounding the particle. A strong interface can first submit the applied stress to the matrix and enhance crazing and then help share with the matrix after crazing; a weak interface would tend to permit easy cavitation at the interface rather than crazing in the matrix, and would be expected to lower the fracture energy. In addition, an ill defined boundary may serve to blunt or slow down growing cracks more effectively; in general, the fracture path tends to proceed through the interfacial region.

An impedance mismatch, i.e., when $\varrho_2 c_2 \gg \varrho_1 c_1$ (c is the velocity of propagation of stress waves), which is common in rubber-modified polymers, tends to create a situation, similar to those caused by imperfect bonding. Indeed, a stress wave practically does not enter the reinforcing particle, but simply circumvents it. The particle in this case only perturbs the stress field by restraining the matrix, provided that the strain is sufficiently high.

Another important role of rubber particles is to initiate branches in very fast cracks. This is because when the crack speed is greater than about one-half the speed of sound in the material under consideration the crack is unable to dissipate enough energy to remain stable so that tends to split into several branches.

The effect of rubber particle content and loading rate on the crack propagation mode has been studied in [29]. The present work, represents an attempt to further our understanding of the behaviour of rubber-modified polymers by using two-dimensional or planar geometries as an analogue to the three-dimensional case. Results of crack propagation mode observation, fracture toughness and crack propagation velocity measurements are presented here. In all cases the method of high speed photography along with the method of dynamic caustics was used.

2. The experimental method of dynamic caustics

The experimental method of dynamic caustics was applied for the study of the influence of inclusions to crack propagations path [30, 31].

A convergent or divergent light beam impinges on the specimen at the close vicinity of the crack tip and the transmitted rays are received on a reference plane, parallel to the plane of the specimen. These rays are scattered and are concentrated along a strongly illuminated curve on the reference plane placed at distance z_0 from the specimen, which is called a "caustic" [32, 33]. From the size and the angular displacement ϕ of the axis of symmetry of the caustic relative to the crack axis, it is possible to calculate the stress intensity factors for the case of mixed-mode conditions by the relations

$$K_I^d = \frac{2(2\pi)^{1/2}}{3z_0 d\lambda_m^{3/2} c_t}\left(\frac{D_t^{max}}{\delta_t^{max}(v)}\right)^{5/2} \quad (1)$$

$$K_{II}^d = K_I^d \tan \tfrac{1}{2}\phi \quad (2)$$

where c_t is the optical constant of the material, d is the thickness of the specimen, λ_m is the magnification ratio of the optical set-up, z_0 is the distance between specimen and reference plane, D_t^{max} is the maximum transverse diameter of the caustic and $\delta_t^{max}(v)$ is a correction factor which depends on the crack velocity. This correction factor is given by nomograms in reference [30].

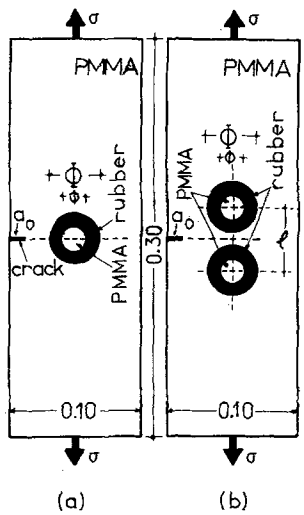

Figure 1 Geometry of specimens. $a_0 = 0.010\,m$, $\phi = 0.023\,m$, $\Phi = 0.034\,m$, $l = 0.046\,m$.

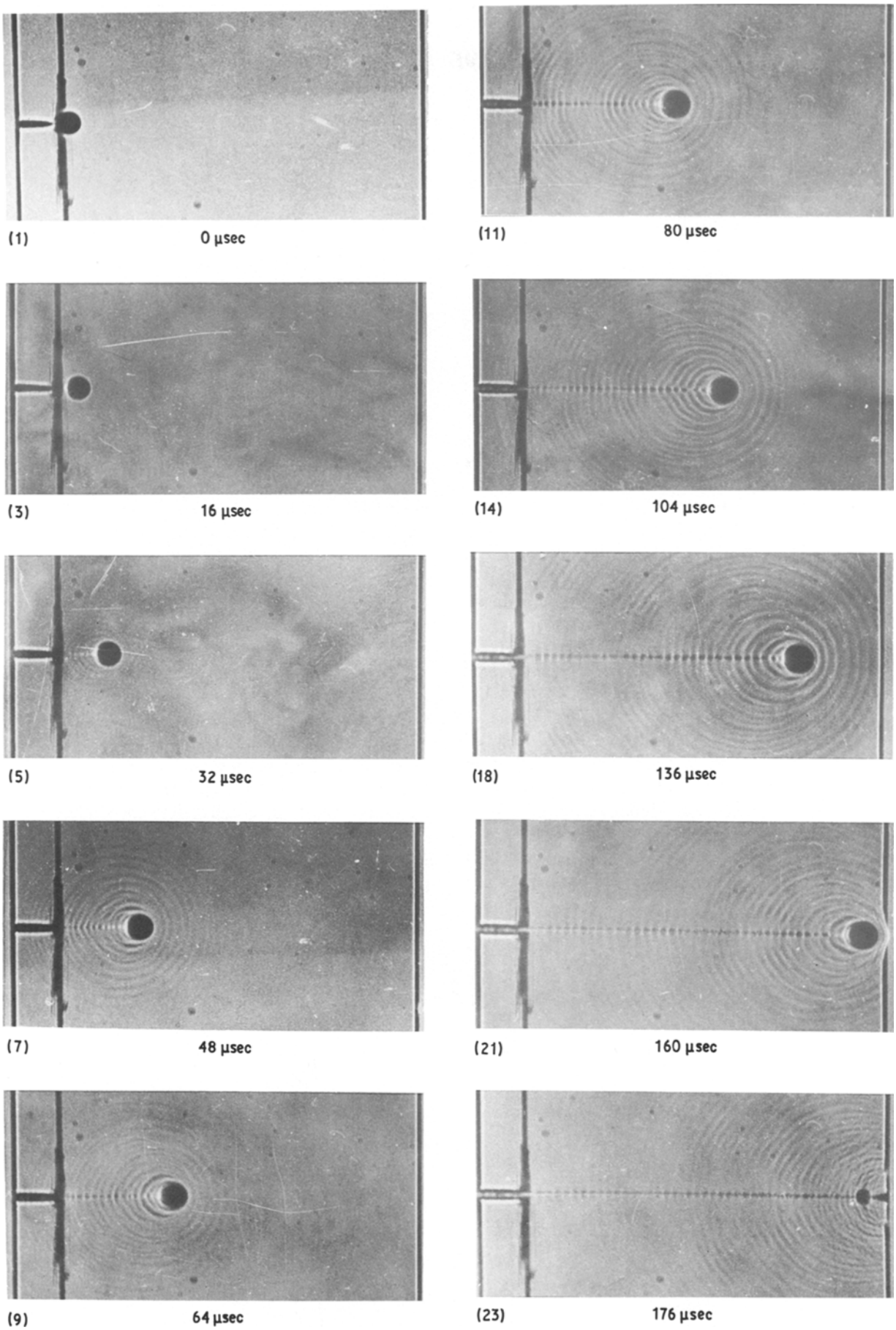

Figure 2 Series of photographs showing the crack propagation in a pure PMMA specimen subjected to a strain rate $\dot{\varepsilon} = 4\,\text{sec}^{-1}$.

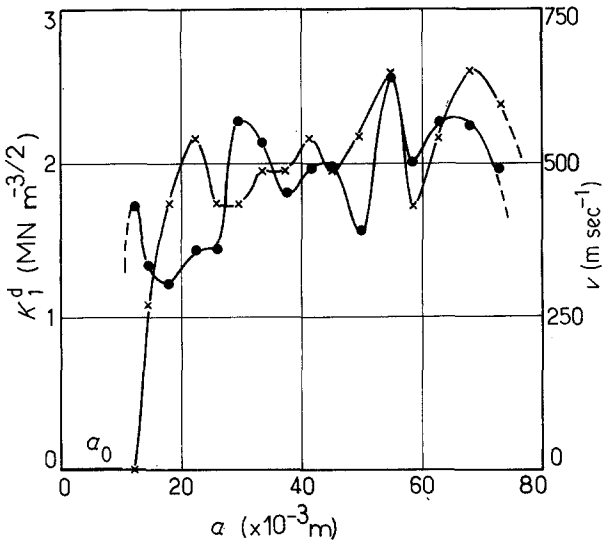

Figure 3 Variation of the stress intensity factor K_I^d (●) and the crack propagation velocity (x), versus the crack length a, for the pure PMMA specimen subjected to a strain rate $\dot{\varepsilon} = 0.8\,\text{sec}^{-1}$.

3. Experimental procedure

The matrix material chosen for the present experimental investigation was in all cases PMMA. The specimens used were in the form of rectangular plates with dimensions $0.30 \times 0.10 \times 0.003\,\text{m}^3$ with an edge artificial crack of length $a_0 = 0.010\,\text{m}$. Three different models were prepared. First, an interference fit was obtained by milling holes in the matrix and press fitting a single or a pair of PMMA circular inclusions. The hole size was nominally 34 mm in diameter. Next, in order to simulate rubber-modified materials, models with circular PMMA inclusions surrounded by concentric rubber rings were prepared. The inclusions diameter was 23 mm whereas the outer diameter of the rubber ring was 34 mm. Finally, models with two holes were prepared. In all cases the inclusions and/or the holes were placed symmetrically to the initial crack direction (Fig. 1).

The specimens were subject to a dynamic tensile load until fracture by Hydropulse High-speed Testing machine of the type of Carl-Schenk Co. with a maximum possible strain rate equal to $\dot{\varepsilon} = 80\,\text{sec}^{-1}$. For the recording of the dynamic-crack propagation a Cranz–Schardin high-speed camera was used disposing 24 sparks with a maximum frequency of 10^6 frames sec^{-1}. In the optical set-up used in the experiments the following quantities were taken: $z_0 = 0.80\,\text{m}$, $\lambda_m = 0.75$. The dynamic properties of PMMA are $E = 4.3 \times 10^9\,\text{N m}^{-2}$, Poisson's ratio $\nu = 0.34$ and stress optical constant $c_t = 0.74 \times 10^{-10}\,\text{m}^2\,\text{N}^{-1}$ [30]. The loading rates applied in the present work were $\dot{\varepsilon} = 0.8$, 2, 4 and $8\,\text{sec}^{-1}$.

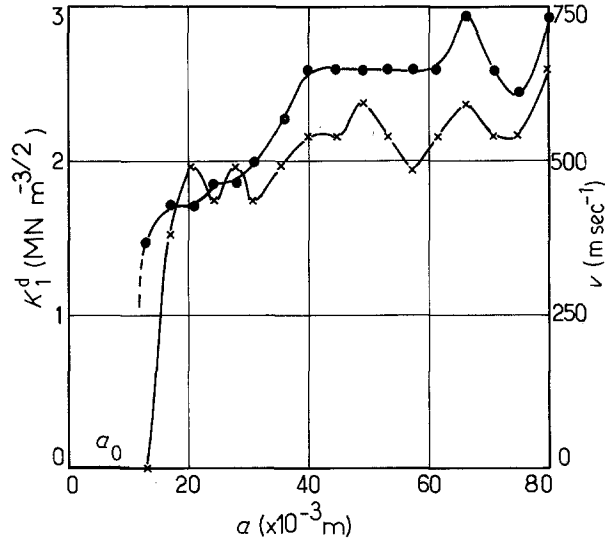

Figure 5 As in Fig. 3 for strain rate $\dot{\varepsilon} = 4\,\text{sec}^{-1}$.

4. Results and discussion

In order to study the influence of interfacial adhesion on the crack propagation path a number of PMMA (matrix) specimens with an edge transverse artificial crack of length $a_0 = 0.010\,\text{m}$ were fractured with strain rates $\dot{\varepsilon} = 0.8$, 2, 4 and $8\,\text{sec}^{-1}$ (Figs 2–6). A number of specimens with a single "complex" inclusion (Fig. 1a) were fractured with strain-rates

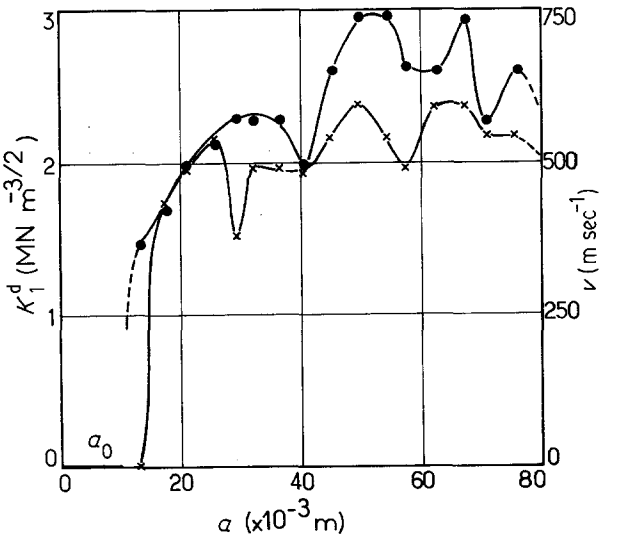

Figure 4 As in Fig. 3 for strain rate $\dot{\varepsilon} = 2\,\text{sec}^{-1}$.

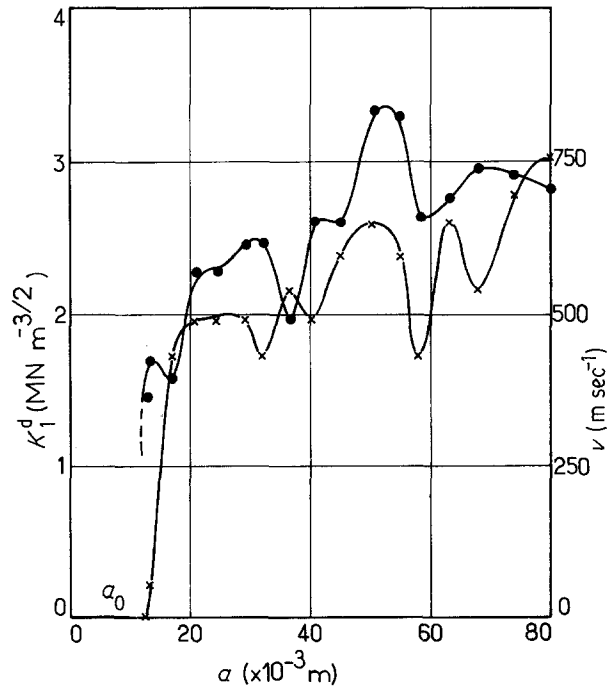

Figure 6 As in Fig. 3 for strain rate $\dot{\varepsilon} = 8\,\text{sec}^{-1}$.

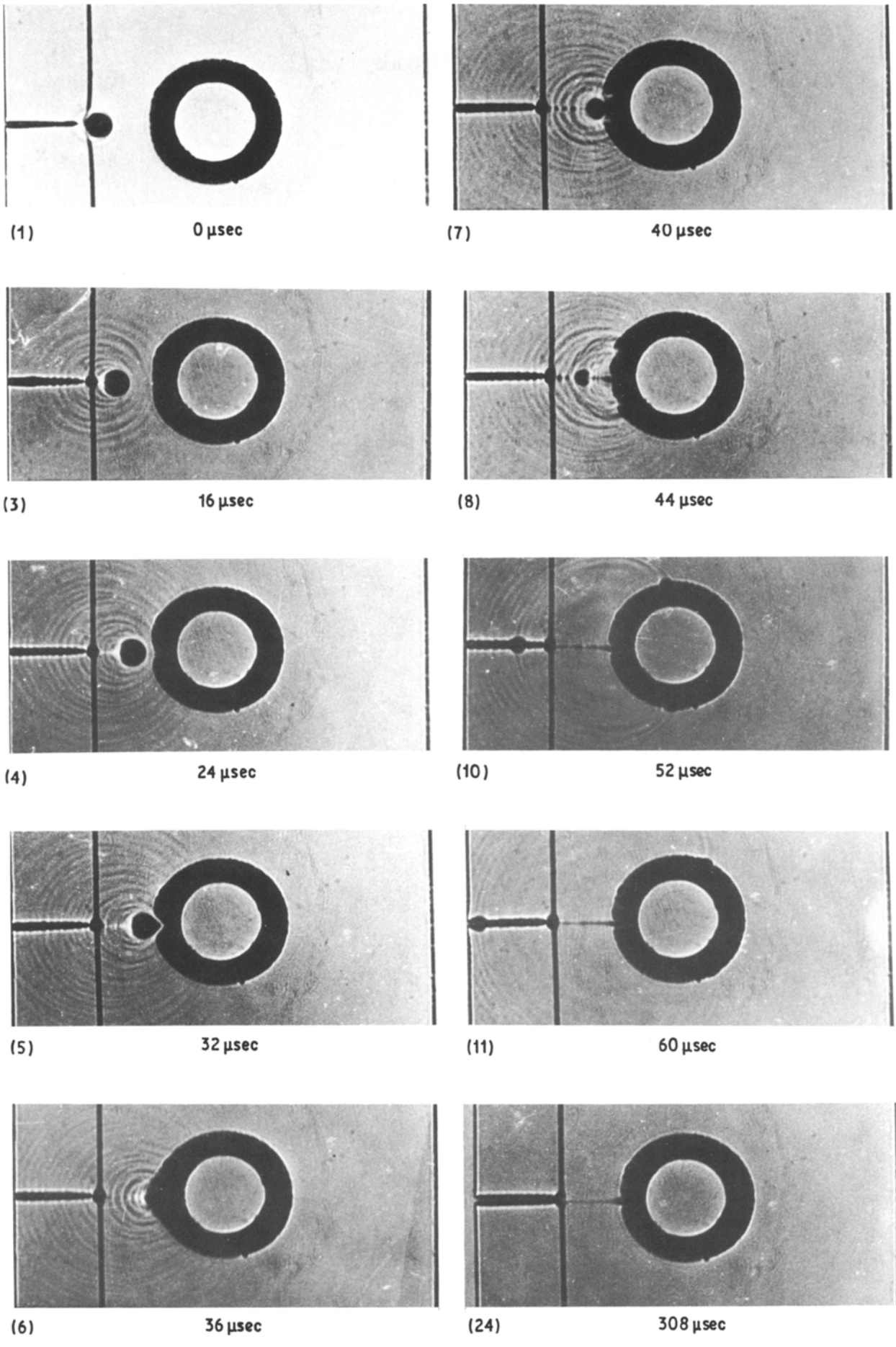

Figure 7 Series of photographs showing the crack propagation in a specimen with a single "complex" inclusion with a rubber interphase, subjected to a strain rate $\dot{\varepsilon} = 4\,\text{sec}^{-1}$.

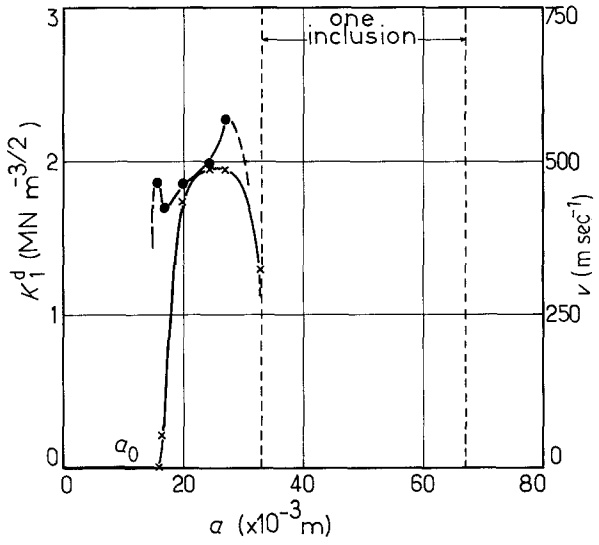

Figure 8 Variation of the stress intensity factor K_I^d and the crack propagation velocity v, versus the crack length a, for the specimen of Fig. 7 subjected to a strain-rate $\dot{\varepsilon} = 4\,\text{sec}^{-1}$.

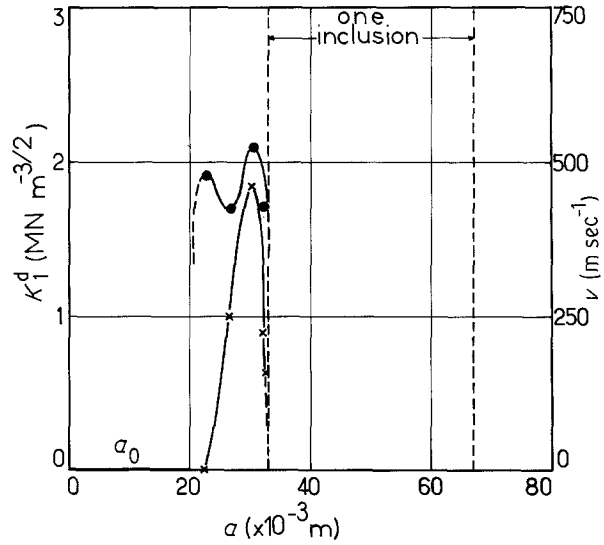

Figure 9 As in Fig. 8 for strain rate $\dot{\varepsilon} = 2\,\text{sec}^{-1}$.

$\dot{\varepsilon} = 2$ and $4\,\text{sec}^{-1}$ and with the initial path on the diametrical axis (Figs 7–9). Also, a number of specimens with a single press-fitting inclusion were fractured with strain-rates $\dot{\varepsilon} = 2$ and $4\,\text{sec}^{-1}$ (Figs 10–12).

The detailed crack propagation process for pure PMMA specimens fractured under a strain-rate $\dot{\varepsilon} = 4\,\text{sec}^{-1}$, may be studied from the series of photographs taken with a Cranz–Schardin high-speed camera and presented in Fig. 2. Next, in order to study strain-rate effects, pure PMMA specimens were fractured under four different strain rates ($\dot{\varepsilon} = 0.8, 2, 4, 8\,\text{sec}^{-1}$). The variation of the crack propagation velocity v and stress intensity factor K_I^d as a function of the crack length a were measured from respective series of photographs and the results are presented in Figs 3 to 6. From these figures it may be observed that an increase in strain rate is followed by a respective increase in crack propagation velocity, which is more pronounced especially in the middle of the crack path, as well as by a relative increase in K_I^d. The continuous emission of stress waves from the tip of the propagating crack as well as the reflections of these waves from the specimens borders (Fig. 2) result in continuous oscillations of the values of both the crack propagation velocity v and K_I^d stress intensity factor.

Fig. 7 presents a series of photographs showing the crack propagation process in a single "complex" inclusion having a rubber interphase. The specimen's geometry is presented in Fig. 1a. This specimen were fractured under a strain rate $\dot{\varepsilon} = 4\,\text{sec}^{-1}$. From the series of photographs it is clear the way the crack approaches the inclusion. As the crack tip approaches the "complex" inclusion an intense deformation of the rubber interphase is observed (Fig. 7, frames 4 and 5). A part of the energy delivered is absorbed by the rubber while the rest is consumed by the reflected stress waves (Fig. 7, frame 8). At the same time the end points of the reflected stress fronts follow symmetrically the rubber–matrix interface and thus forming an interface crack path. After a period of time (arrest time) an amount of energy is concentrated at the antidiametrical point and the crack start propagating again in the matrix material. The crack arrest time in the present case was 172 μsec and it depends on the nature and quality of the bond that exist between rubber and matrix. The variation of the stress intensity factor K_I^d and the crack propagation velocity v as a function of the crack length a for the single "complex" inclusion specimen and for strain rate $\dot{\varepsilon} = 2\,\text{sec}^{-1}$ is given in Fig. 8. The variation of the same quantities for the same kind of specimen but for $\dot{\varepsilon} = 4\,\text{sec}^{-1}$ is given in Fig. 9. In these figures dotted lines show the extent of the inclusion. It may be observed that when the crack tip approaches the inclusion both v and K_I^d attain a maximum value and subsequently afterwards an abrupt decrease is observed. Next, the main crack stops momentarily while the interface crack propagates around the inclusion. During this time interval there is no principal crack propagation effect and a crack arrest is achieved. A great part of the energy is absorbed by the rubber interphase and there is not any energy transmission to the PMMA inclusion. Thus the role of the rubber interphase is to protect the main inclusion from the effect of the stress waves developed due to the crack propagation process. The degree of this protection depends on the quality of adhesion and the degree of compatibility of the constituent materials. Similar phenomena are also observed in the case where a press-fitting inclusion is used instead of the "complex" inclusion.

Fig. 10 presents a series of photographs showing the crack propagation process in a specimen with a PMMA press-fitting inclusion fractured under strain-rate $\dot{\varepsilon} = 4\,\text{sec}^{-1}$. The crack arrest time in this case is 464 μsec which is greater than that in the case of the specimen with a single "complex" inclusion. From these photographs we may observe an oscillation of the interface area which follows the reflection of the stress waves from both the matrix-inclusion interface and the specimens borders. Indeed, this phenomenon may be observed twice: the first time in frames 9 to 17 having a duration of 260 μsec, and the second time in frames 17 to 22 having the same duration of 260 μsec.

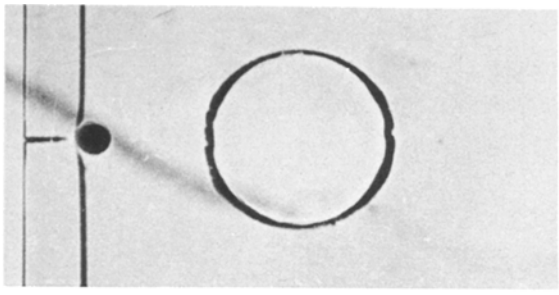

(1) 0 μsec

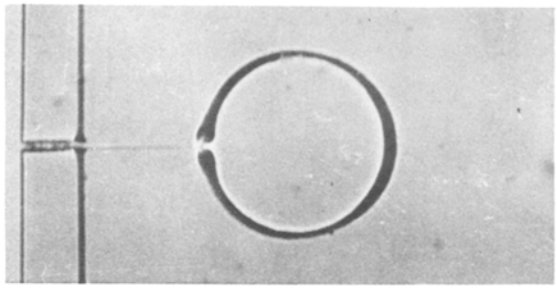

(12) 200 μsec

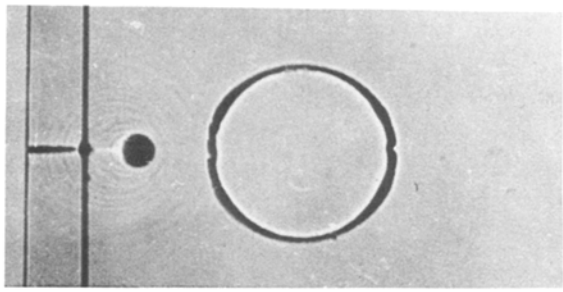

(4) 24 μsec

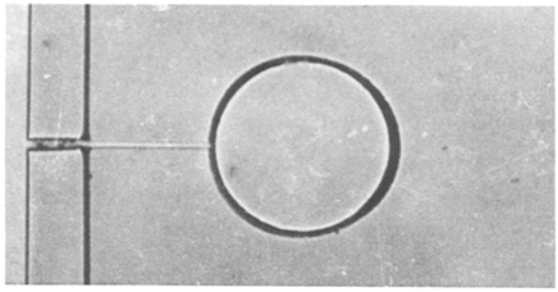

(17) 360 μsec

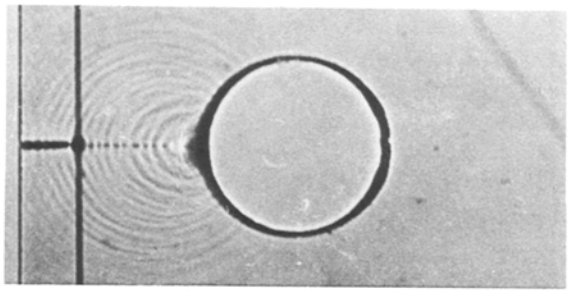

(6) 56 μsec

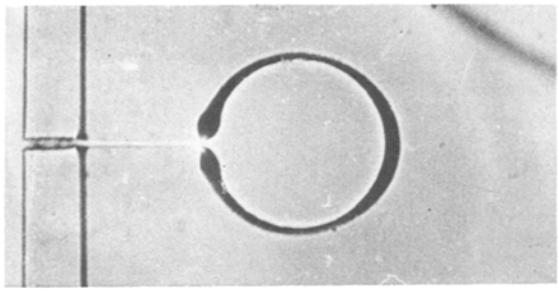

(19) 424 μsec

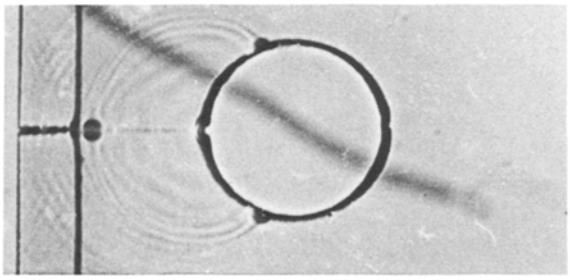

(7) 72 μsec

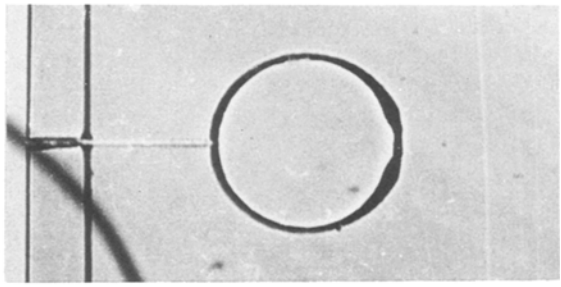

(22) 520 μsec

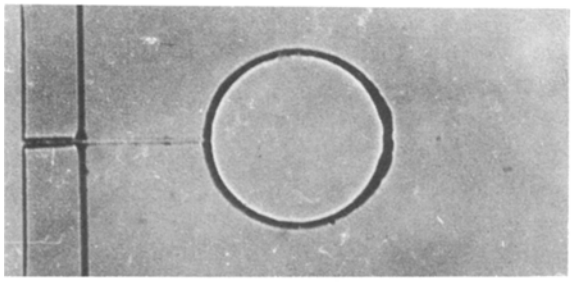

(9) 104 μsec

Figure 10 Series of photographs showing the crack propagation in a specimen having one press-fitting PMMA inclusion. The strain rate was $\dot{\varepsilon} = 4\,\text{sec}^{-1}$.

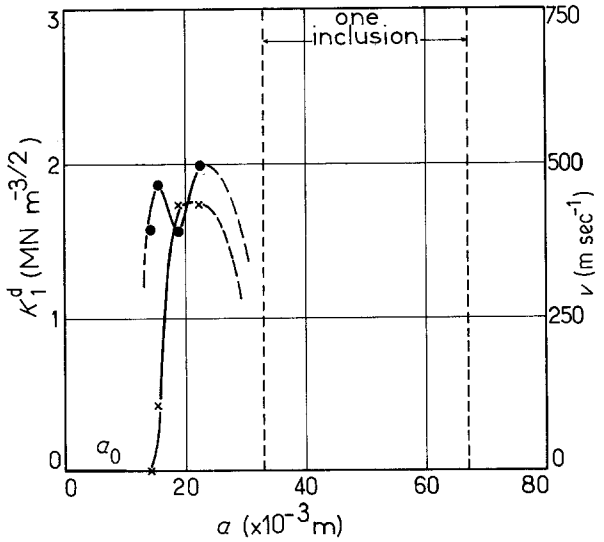

Figure 11 Variation of the stress intensity factor K_I^d and the crack propagation velocity v, with the crack length a, for a specimen having one press-fitting PMMA inclusion and for strain rate $\dot{\varepsilon} = 2\,\text{sec}^{-1}$.

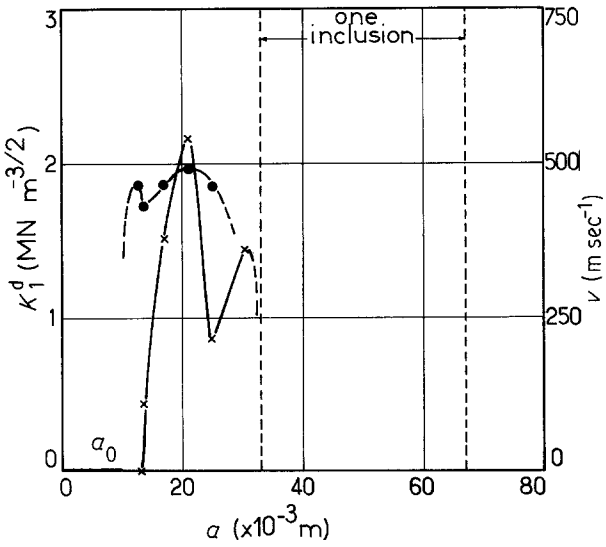

Figure 12 As in Fig. 11 for strain rate $\dot{\varepsilon} = 4\,\text{sec}^{-1}$.

A characteristic phenomenon observed in frame 22 is the intense deformation of the antidiametric point. From this point the crack will start to propagate into the matrix after it has followed the matrix-inclusion interface.

Fig. 11 shows the variation of crack propagation velocity v as well as that of the stress intensity factor K_I^d as a function of crack length a and for strain-rate $\dot{\varepsilon} = 2\,\text{sec}^{-1}$ while the variation of the same quantities for $\dot{\varepsilon} = 4\,\text{sec}^{-1}$ is shown in Fig. 12. The crack approaches the inclusion in a way similar to that observed in the case of the rubber interphase.

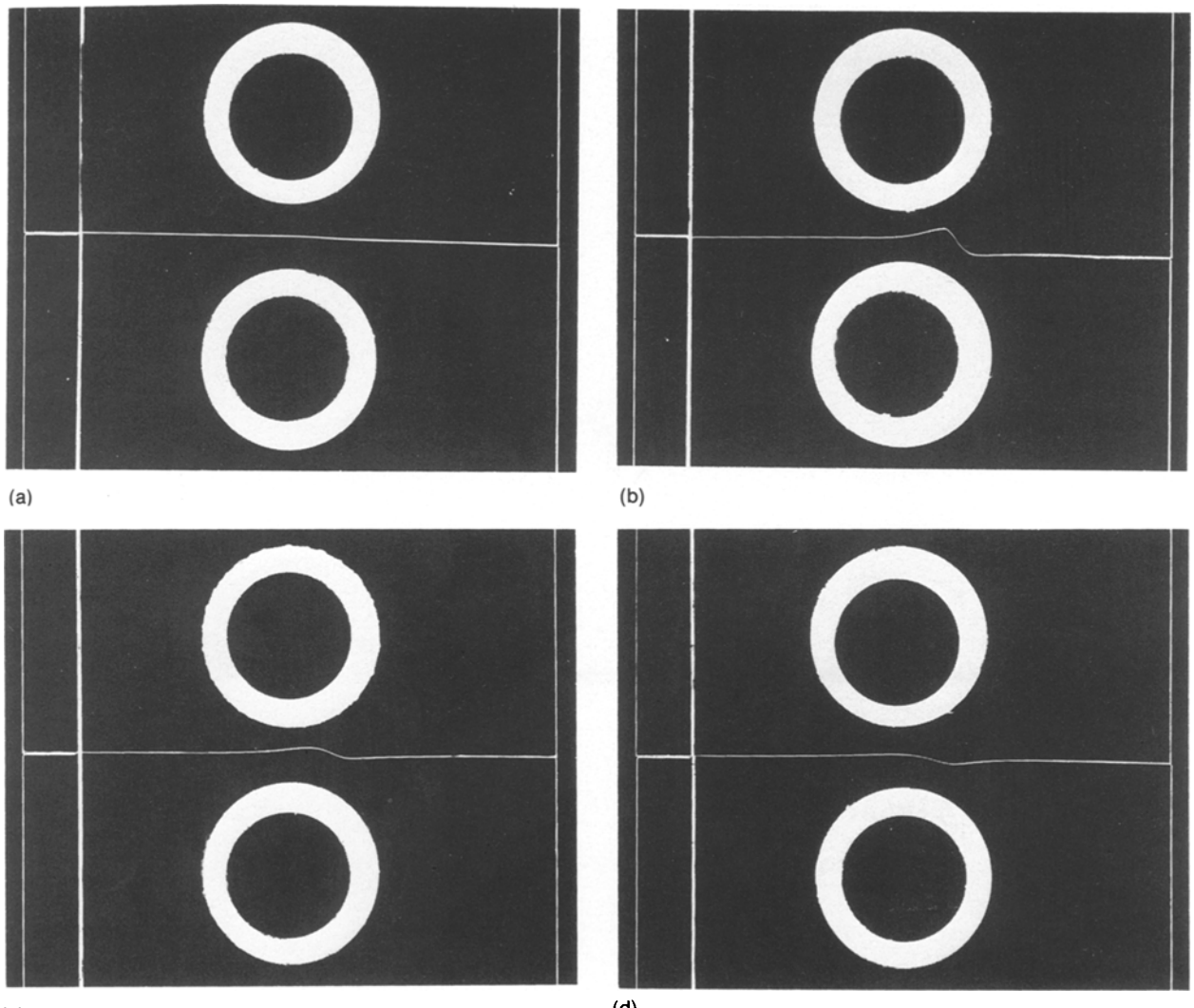

Figure 13 Photographs showing crack propagation in specimens having two "complex" inclusions with a rubber interphase. The strain-rates were (a) $\dot{\varepsilon} = 0.8\,\text{sec}^{-1}$ (b) $\dot{\varepsilon} = 2\,\text{sec}^{-1}$ (c) $\dot{\varepsilon} = 4\,\text{sec}^{-1}$ and (d) $\dot{\varepsilon} = 8\,\text{sec}^{-1}$.

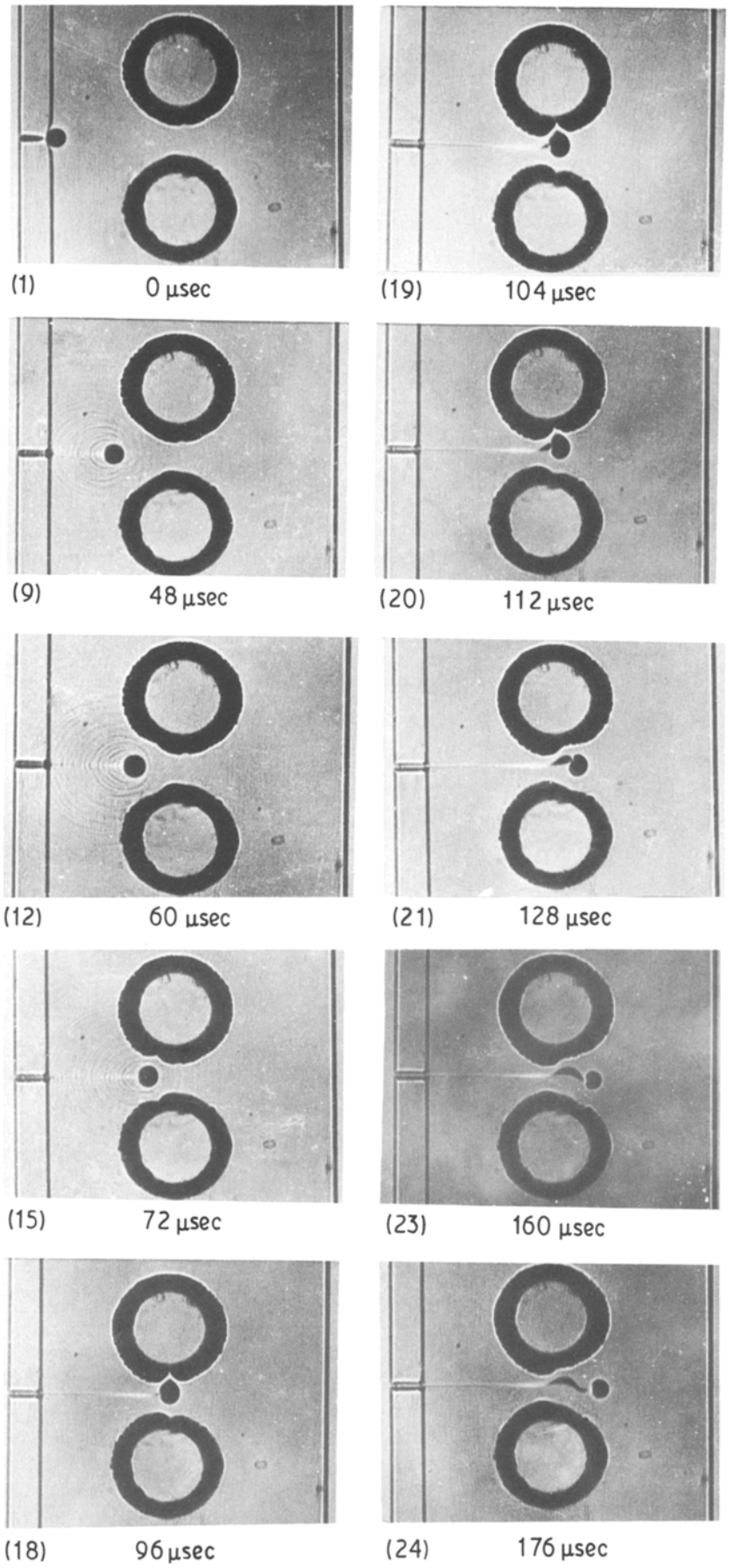

Figure 14 Series of photographs showing the crack propagation in specimen of Fig. 13c.

Next, in order to study the effect of filler–filler interactions as well as strain-rate effects, specimens with two "complex" inclusions at constant inter-inclusion separation (Fig. 1b) were fractured under four different strain rates.

Fig. 13 shows typical crack path of four such specimens fractured under four different strain rates. From these photographs it may be observed that for low strain rate ($\dot{\varepsilon} = 0.8\,\text{sec}^{-1}$) the crack path is an almost straight line showing an independence on the

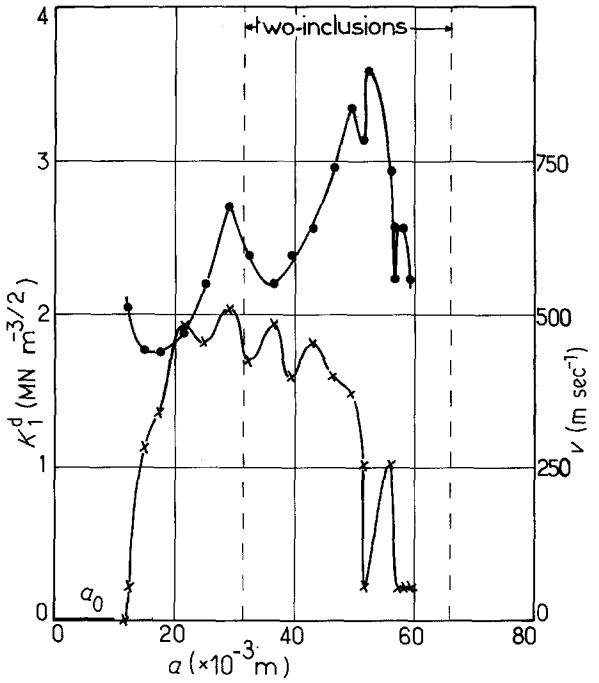

Figure 15 Variation of the stress intensity factor K_I^d and the crack propagation velocity v, versus the crack length a, for the specimen of Fig. 13b.

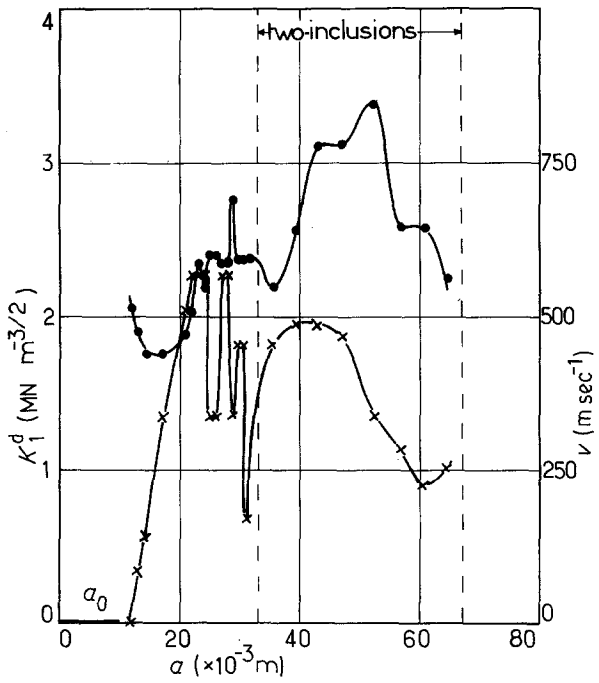

Figure 17 As in Fig. 12 for the specimen of Fig. 13d.

existence of the two inclusions. This may be due to the fact that at very slow strain rates the viscoelastic processes are greatly reduced and the crack propagation process is controlled mainly by the elastic equilibrium properties of the materials. At higher applied strain rates where viscoelastic processes are more pronounced, a kink in the crack path at the interparticle area is observed showing a stronger effect of the fillers on the crack propagation process. However, it is very interesting to note that this kind of behaviour was always more pronounced in the case where $\dot{\varepsilon} = 2\,\text{sec}^{-1}$ while for the higher strain rate ($\dot{\varepsilon} = 4$ and $8\,\text{sec}^{-1}$), this kink was reduced in depth.

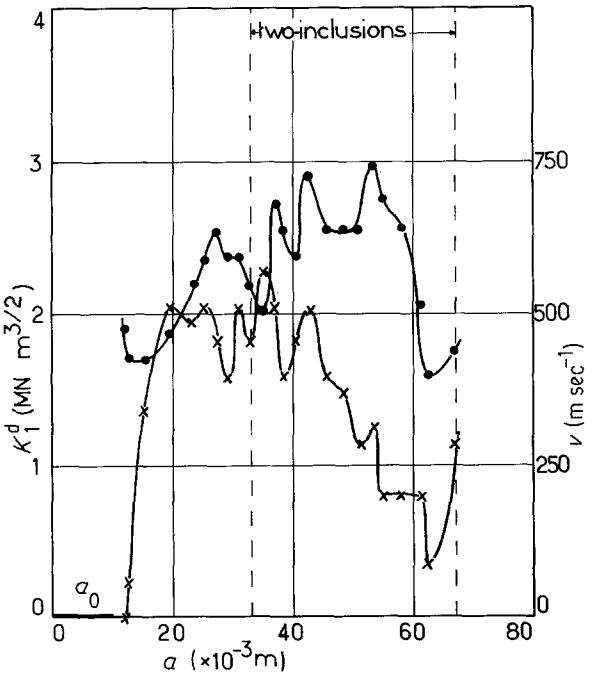

Figure 16 As in Fig. 12 for the specimen of Fig. 13c.

The detailed crack propagation process for the case of two inclusions and for strain rate $\dot{\varepsilon} = 4\,\text{sec}^{-1}$ is shown in the series of photographs presented in Fig. 14. From these photographs the evaluation of the instantaneous velocities of the propagation crack was derived, while from the geometric characteristics of the respective caustics the dynamic stress intensity factor K_I^d was evaluated by using relation 1. Also, in these photographs the whole crack propagation process in the area between the two inclusions may be observed in detail as well as the effect of the presence of the inclusions on the crack propagation velocity and the stress field developed at the tip of the crack. In the interparticle area the observed crack propagation delay is of the order of 112 μsec (frames 9–23 in Fig. 14). Specifically in frames 18–20 a more pronounced effect of the inclusions on the crack propagation process is observed which results in the development of a kink.

The variation of the crack propagation velocity v as well as that of the stress intensity factor K_I^d as a function of crack length a for strain rates $\dot{\varepsilon} = 2, 4$ and $8\,\text{sec}^{-1}$ is shown in Figs 15, 16 and 17 respectively. From these figures it may be observed that the crack propagation velocity is strongly affected from the presence of the two inclusions and this is more pronounced in the interparticle area. Indeed, especially for the case of $\dot{\varepsilon} = 2\,\text{sec}^{-1}$ (Fig. 15), as the crack propagates in the interinclusion area, the crack propagation velocity decreases having too low a minimum value. For strain rate $\dot{\varepsilon} = 8\,\text{sec}^{-1}$, where the crack path is strongly affected by the presence of the inclusions and the observed kink is not very deep (Fig. 13a), the crack propagation velocity in the interinclusion area increases at first and subsequently decreases (Fig. 17). The respective variation of the stress intensity factor K_I^d shows an increase which is more pronounced in the interinclusion area where

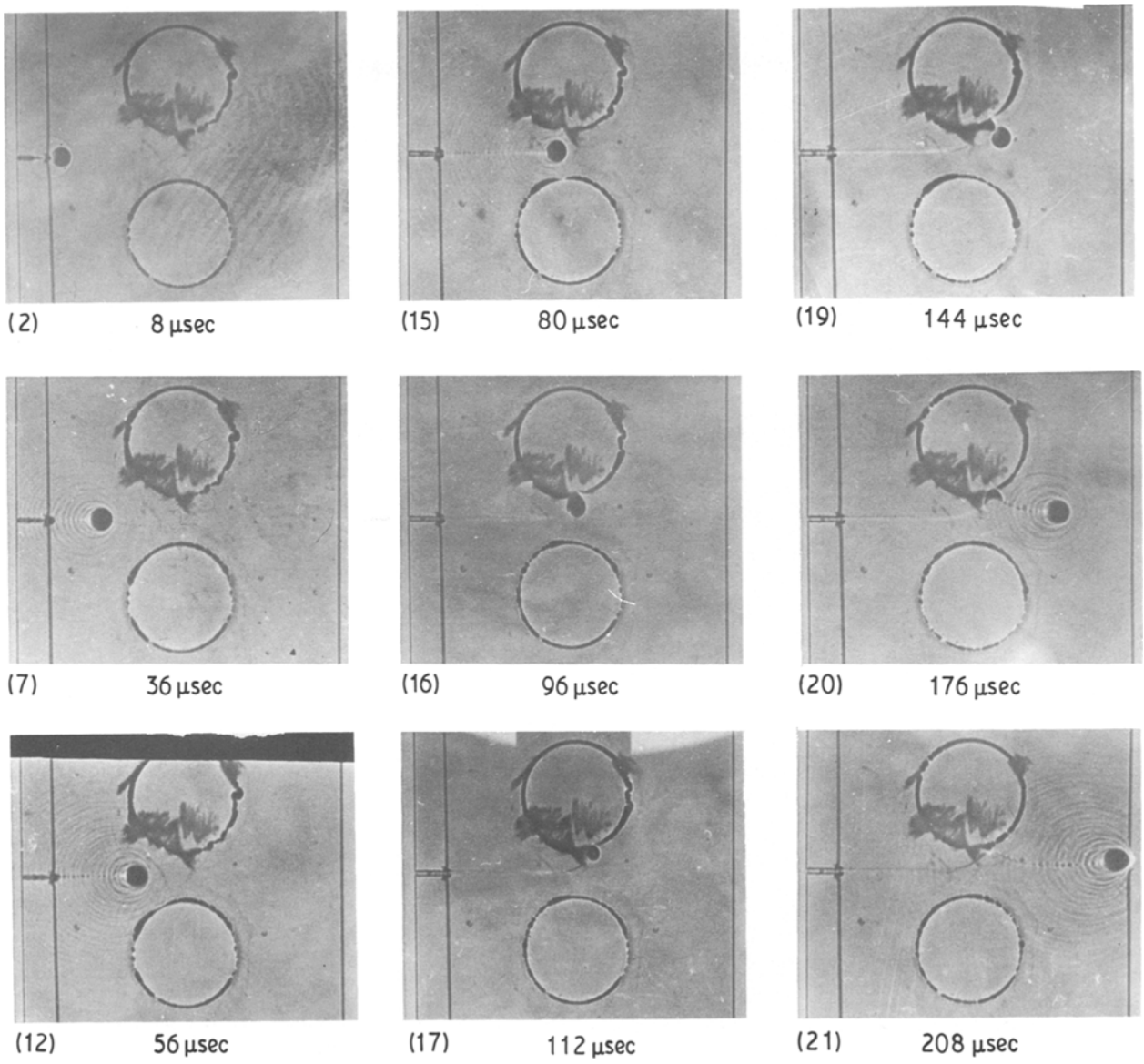

Figure 18 Series of photographs showing the crack propagation in a specimen having two press-fitting PMMA inclusions. The strain rate was $\dot{\varepsilon} = 4\,\text{sec}^{-1}$.

crack propagation velocity tends to zero and this case is almost similar to that of a static one.

The attraction of the crack by one of the inclusions and the development of the kink (Fig. 14) strongly depends on the relative eccentricity of the initial notch. The crack propagation process in the inter-particle area is characterized by the attraction of the crack by one of the inclusions and the absorption of a great part of the crack propagation energy by the rubber interphase. Because of this absorption the crack is not permitted to propagate through the inclusion.

The same effects, but not so strong, are observed in the case of press-fitting inclusions. Fig. 18 presents a series of photographs showing the detailed crack propagation process for the case of two press-fitting inclusions. As the crack propagates into the inter-inclusion area it shows a crack delay of about 88 μsec (Fig. 18, frames 12 to 19). This crack delay is lower than the respective one observed in the case of two inclusions with a rubber interphase (Fig. 14). Also, the

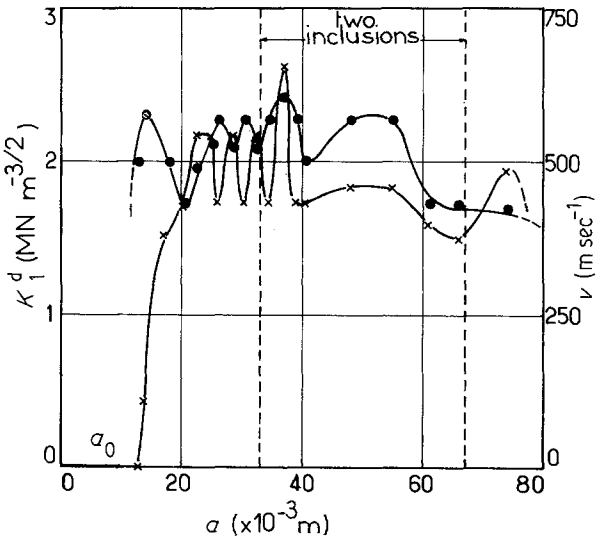

Figure 19 Variation of the stress intensity factor K_I^d and the crack propagation velocity v, with the crack length a, for a specimen having two press-fitting PMMA inclusions and for a strain-rate $\dot{\varepsilon} = 0.8\,\text{sec}^{-1}$

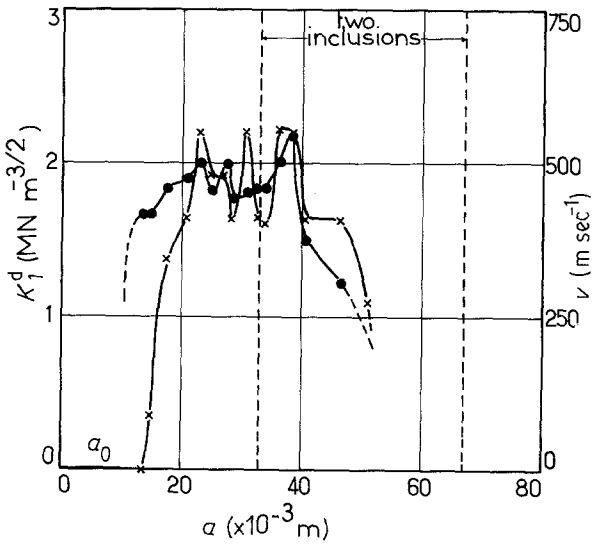

Figure 20 As in Fig. 19 for strain rate $\dot{\varepsilon} = 2\,\text{sec}^{-1}$.

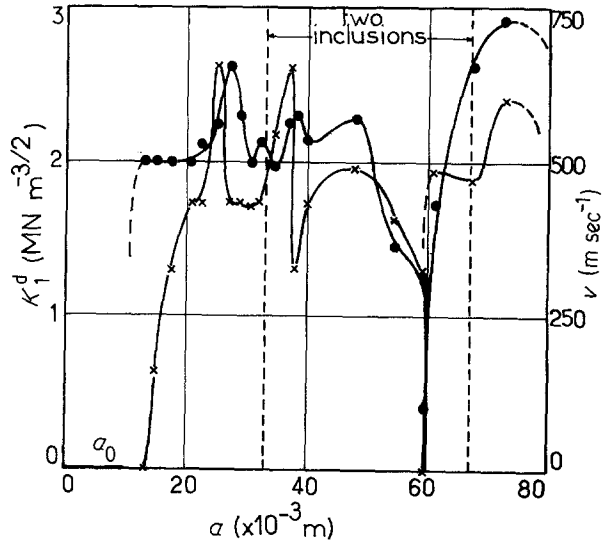

Figure 21 As in Fig. 19 for strain rate $\dot{\varepsilon} = 4\,\text{sec}^{-1}$.

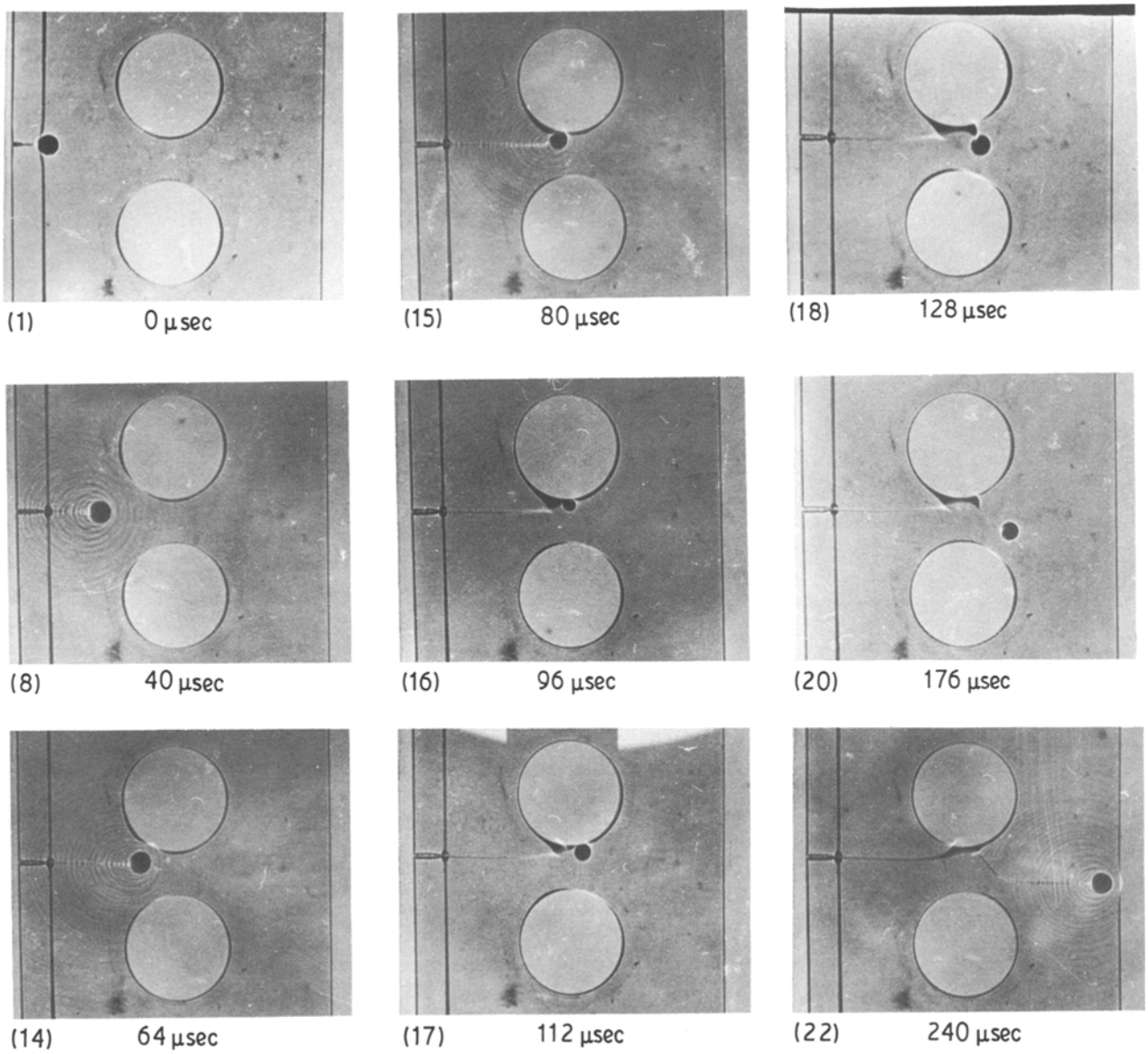

Figure 22 Series of photographs showing the crack propagation in a specimen having two holes subjected to a strain rate $\dot{\varepsilon} = 2\,\text{sec}^{-1}$.

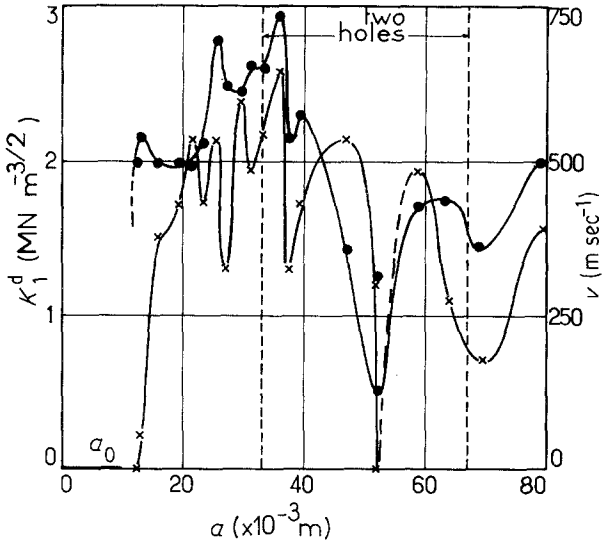

Figure 23 Variation of the stress intensity factor K_I^d and the crack propagation velocity v, with the crack length a, for a specimen having two holes subjected to a strain rate $\dot{\varepsilon} = 2\,\text{sec}^{-1}$.

kink developed in this case is much more abrupt than in the case of the rubber interphase since the energy absorbed by the PMMA inclusion is much lower than the respective one absorbed by the rubber interphase.

The variation of the crack propagation velocity v and that of the stress intensity factor K_I^d as a function of the crack length a and for strain rates $\dot{\varepsilon} = 0.8$, 2 and $4\,\text{sec}^{-1}$ is shown in Figs 19, 20 and 21 respectively. These variations are more intense than in the case of the rubber interphase, while at the point where the kink is developed a crack arrest of about 20 μsec (Fig. 18, frames 16 and 17) is observed which was not observed in the case of the rubber interphase. Immediately after the crack momentarily stops at the matrix-inclusion interface (Fig. 18, frame 17) a reinitiation of the crack is observed while the crack propagation velocity increases again (Fig. 21).

Finally, for the sake of comparison, an additional experiment was conducted with specimens having two holes drilled in places corresponding to those of the inclusions in the previous experiments. Fig. 22 presents a series of photographs showing the crack propagation process in the case of a specimen with two holes. In this case the crack delay time observed during the crack propagation in the interhole area was of the order of 64 μsec (Fig. 22, frames 14 to 18), while the crack arrest time during the development of the kink (Fig. 22, frames 15 to 17) was about 32 μsec. Fig. 23 shows the variation in the crack propagation velocity v and the respective variation of the stress intensity factor K_I^d as a function of the length a of the propagating crack and for strain rate $\dot{\varepsilon} = 2\,\text{sec}^{-1}$. These variations are very intense especially as the crack enters the interhole area.

5. Conclusions

The dynamic fracture behaviour of several rubber-modified composite models has been studied. The results of the present study may be summarized as follows.

(i) For the pure PMMA specimens an increase in strain rate is followed by a respective increase in crack propagation velocity.

(ii) In the case of single "complex" inclusion, as the crack approaches the inclusion an intense deformation of the rubber interphase and an interface crack path were observed. Also due to the energy absorbed by the rubber interphase crack delay and in some cases crack arrest phenomena were observed.

(iii) An oscillation of the interface area has been observed in the case of a single press-fitting inclusion while the crack arrest time was about 464 μsec.

(iv) In the case of specimens with two "complex" inclusions it was found that at low strain rates the crack path is almost straight while at higher strain rates a kink was observed in the interparticle area which was more pronounced for $\dot{\varepsilon} = 2\,\text{sec}^{-1}$. Also in the same area there is an intense variation of both v and K_I^d the degree of which depended on the strain rate.

(v) Similar effects have been observed in the case of two press-fitting inclusions and/or two holes the difference being on the degree of variation of v and K_I^d as well as on the depth of the kink developed in the interparticle area.

References

1. C. B. BUCKNALL, "Toughened Plastics" (Applied Science, London, 1977).
2. S. NEWMAN, in "Polymer Blends", Vol. 2, edited by D. R. Paul and S. Newman (Academic, New York, 1978) Ch. 13.
3. R. P. BURFORD and M. PITTOLO, *J. Mater. Sci.* **21** (1986) 2308.
4. M. PITTOLO and R. P. BURFORD, *ibid.* **21** (1986) 1769.
5. *Idem, Rubber Chem. Technol.* **58** (1985) 97.
6. G. RIES, M. SCHLIENGER and S. MARTIN, *J. Macromol. Sci. (Phys.)* **B17** (1980) 355.
7. A. ECHTER, *Angew. Macromol. Chem.* **58/59** (1977) 175.
8. C. B. BUCKNALL, F. F. P. CÔTE and I. K. PARTRIDGE, *J. Mater. Sci.* **21** (1986) 301.
9. C. B. BUCKNALL, P. DAVIES and I. K. PARTRIDGE, *ibid.* **21** (1986) 307.
10. R. P. KAMBOUR, *J. Polym. Sci.* **A2** (1964) 4159.
11. O. K. SPURR and W. D. NIEGISH, *J. Appl. Polym. Sci.* **6** (1962) 585.
12. D. G. GRAND, R. P. KAMBOUR and W. F. HAAF, *J. Polym. Sci. A-2* **10** (1972) 1565.
13. E. H. MERZ, G. C. CLAVER and M. BAIER, *ibid.* **22** (1956) 325.
14. J. A. SCHMITT and H. KESKKULA, *J. Appl. Polym. Sci.* **3** (1960) 132.
15. S. NEWMAN and S. STRELLA, *ibid.* **9** (1965) 2297.
16. K. DINGES and H. SCHUSTER, *Makromol. Chem.* **101** (1967) 200.
17. R. P. KAMBOUR, *J. Polym. Sci., Macromol. Rev.* 7 (1973) 112.
18. C. F. PARSONS and E. L. SUK, *Chem. Ser.* **99** (1971).
19. R. D. SUDDUTH, *J. Appl. Polym. Sci.* **22** (1978) 2427.
20. G. C. PAPANICOLAOU, S. A. PAIPETIS and P. S. THEOCARIS, *Colloid Polym. Sci.* **256** (1978) 689.
21. G. C. PAPANICOLAOU and P. S. THEOCARIS, *ibid.* **257** (1979) 239.
22. P. S. THEOCARIS and G. C. PAPANICOLAOU, *Fibre Sci. Technol.* **12** (1979) 421.
23. G. C. PAPANICOLAOU, P. S. THEOCARIS and G. D. SPATHIS, *Colloid Polym. Sci.* **258** (1980) 1231.
24. P. S. THEOCARIS, G. C. PAPANICOLAOU and G. D. SPATHIS, *Fibre Sci. Technol.* **15** (1981) 187.
25. P. S. THEOCARIS, E. P. SIDERIDIS and G. C. PAPA-

NICOLAOU, *J. Reinforced Plastics and Composites* **4** (1985) 396.
26. E. P. SIDERIDIS, P. S. THEOCARIS and G. C. PAPANICOLAOU, *Rheologica Acta* **25** (1986) 350.
27. C. D. PAPASPYRIDES, G. C. PAPANICOLAOU and T. DUVIS, *Mater. Chem. Phys.* **17** (1987) 531.
28. G. C. PAPANICOLAOU and C. D. PAPASPYRIDES, *ibid.* **17** (1987) 453.
29. J. MILIOS, G. C. PAPANICOLAOU and R. J. YOUNG, *J. Mater. Sci.* **21** (1986) 4281.
30. P. S. THEOCARIS and G. A. PAPADOPOULOS, *Engng Fract. Mech.* **13** (1980) 683.
31. *Idem., ASTM STP* **971** (1983) II–320.
32. P. S. THEOCARIS, *J. Appl. Mech.* **37**, ASME Vol. 92, Series E (1970) 409.
33. *Idem.*, "Development in Stress Analysis ", Vol. 1, edited by G. Holister (1979) 27. Ch. 2.

Received 23 September 1987
and accepted 26 January 1988